The Microphysics of the Warm-rain and Ice Crystal Processes of Precipitation in Simulated Continental Convective Storms

Ashok Gupta (ashok.k.gupta@vanderbilt.edu)
Vanderbilt University https://orcid.org/0000-0002-2282-7266
Vaughan Phillips
Deepak Waman
Sachin Patade
Akash Deshmukh
Arti Jadav
Aaron Bansemer
National Center for Atmospheric Research (NCAR) https://orcid.org/0000-0002-3714-1099

Article

Keywords:

Posted Date: May 13th, 2022

DOI: https://doi.org/10.21203/rs.3.rs-1603291/v1

Version of Record: A version of this preprint was published at Communications Earth & Environment on June 27th, 2023. See the published version at https://doi.org/10.1038/s43247-023-00884-5.

Abstract

Precipitation is fundamental to the hydrological cycle. There are two possible mechanisms for its formation in clouds generally: the "warm-rain process" and the "ice crystal process". This study uses a microphysically advanced aerosol-cloud (AC) model to understand the contributions from the warm (from the warm-rain process) and cold (from the ice crystal process) components of the surface precipitation in a pair of contrasting convective storms that are cold-based (STEPS) and slightly warm-based (MC3E). Tagging-tracer techniques enabled analysis of microphysical pathways leading to the simulated precipitation.

The cold components of graupel and rain mass are higher than the corresponding warm components in both simulations of the STEPS and MC3E storms. About ~80% of accumulated surface precipitation is predicted to originate from ice-crystal process in both cases. In sensitivity tests with lowering of cloud base to warmer levels near the ground, the origin of most of the surface precipitation is switched to the warm-rain process in both cases, even though precipitation is mostly in the ice-phase aloft. This is reinforced by inclusion of maritime solute aerosol conditions additionally. In conclusion, this study explains the distinct behavior of precipitation processes in the cold-base and warm-base convective clouds.

Preface

This study has discovered that both the warm-rain and ice crystal processes of precipitation co-exist in any given storm, and the balance between both is determined by cloud base temperature and solute aerosol conditions.

Introduction

Motivation for this study

Precipitation is fundamental to the hydrological cycle and is a major sink for condensate mass in clouds, controlling the cloud lifetime and the cloud-radiation feedbacks in climate change[1]. In a warming climate, the increased rates of heavy convective precipitation, with uneven distribution over land and ocean, have already been observed in the extratropics[2,3]. These patterns are influenced by various microphysical pathways, such as raindrop freezing, aggregation of ice and its melting. There is a lack of detail in the representation of these microphysical pathways for precipitation in global climate models, affecting climate change projections[2].

Precipitation processes

Both cloud microphysical and macrophysical processes, along with the environmental conditions, regulate the intensity, scales, and timing of precipitation[4,5,6,7,8,9,10,11]. There are two essential microphysical processes to form precipitation:

1. *Warm-rain process*: cloud droplets collide and coalesce to form ("warm") raindrops that then grow by more coalescence and may freeze to form ("warm") graupel, which may then melt during fallout.
2. *Ice crystal process:* ice crystals can be formed by heterogeneous ice nucleation, and their growth can create snow (e.g., aggregates), which may rime to form ("cold") graupel. Again, this ice precipitation may melt to form ("cold") rain.

In nature, both the warm-rain and ice-crystal processes of precipitation can co-exist, being interlinked, making their evolution a complex process. For example, in point 1, the raindrops freezing can occur in raindrop-ice collisions[12,13,14,15,16]. For the same initial mass, a graupel particle is more efficient at accretion of cloud mass for precipitation growth relative to a liquid drop[17].

Most global climate models are not equipped to track precipitation components associated with the warm-rain and ice crystal processes rigorously. So, their precise balance globally is uncertain.

Misconceptions about precipitation types

Misconceptions can easily arise from the fact that the ice phase of clouds can be forced by either the warm-rain process or the ice crystal process. The mere existence of ice precipitation does not necessarily imply that most of its mass is from the ice crystal process, although active ice nuclei initiated it. In reality, most of the mass of ice precipitation in a given slightly warm-based cloud may sometimes be from the warm-rain process including raindrop freezing[15,18]. Therefore, the assumption that surface precipitation must be cold merely due to the presence of ice somewhere aloft in the cloudy column may not always be valid. Such an assumption was adopted in some satellite-based and global modeling studies[19,20], which might affect determination of warm rain occurrence over the globe. It is an open question as to what are the circumstances by which warm precipitation prevails when clouds are deep.

Environmental factors influencing precipitation types

There are many ways in which the environment controls surface precipitation. Firstly, the warm-rain process requires that cloud droplets attain a critical average size (~20 microns) such that the collision efficiency permits coalescence[21,22]. The adiabatic liquid water content (LWC) must be large enough and cloud droplets not too numerous. Conversely, the ice crystal process requires a cloud top cold enough for primary ice formation. A key factor regulating the balance between the warm-rain process and ice-crystal process is the environmental relative humidity in the lower troposphere, which controls the temperature of cloud base and collision-coalescence. For instance, Fan et al.[23] reported that raising the cloud base drastically diminished the sensitivity of precipitation with respect to cloud condensation nuclei (CCN) due to suppression of the CCN-sensitive warm-rain process.

Secondly, regarding the cloud glaciation, there are many mechanisms of fragmentation of ice[24]. The growth of ice crystals via riming can produce a copious amount of secondary ice particles in slightly

warm-based clouds[18,25,26,27]. These ice particles secondary ice production (SIP) influence surface precipitation[6,27].

Figure 1 highlights these microphysical processes controlling warm-rain (red line) and ice crystal (blue line) processes of precipitation. The contributions from warm and cold precipitation to the total surface precipitation are determined by several interactions between hydrometeor species via processes, such as coalescence, riming, deposition, and sublimation. Some of these are temperature dependent. For instance, the melting of snow and cold graupel from the growth of ice crystals (Fig. 1) causes cold rain. Note that here the terms "warm" and "cold" do not refer to temperature and denotes only whether the warm-rain or ice-crystal processes cause the precipitation.

Supercooled rain in slightly warm-based and cold-based convective clouds

Aircraft observations in slightly warm-based convective clouds show supercooled rain just before the onset of glaciation[13,26,28,29] with raindrops freezing as observed by radar[12]. Very rapid growth of concentrations of ice by many orders of magnitude during the initial raindrop freezing is seen. These frozen drops melt to form rain with the ice-phase controlled by coalescence of the liquid-phase[14,15,18,30]. By contrast, no supercooled rain was detected by aircraft in cold-based convective (cloud base was at about ~0^{o}C) clouds during the Severe Thunderstorms Electrification and Precipitation Study (STEPS) campaign on 19/20 June 2000 in the US High Plains. This STEPS observation is a typical example of a prevailing ice crystal process without appreciable coalescence.

Numerical modeling offers a way to analyze causation in natural clouds and the relative strengths of such microphysical pathways of precipitation[10, 27, 31,32,33,34,35,36,37,38]. Thus, the present study follows a modeling approach.

Aerosol-Cloud (AC) modeling: two field observations of convective storms

In our aerosol-cloud (AC) model with hybrid bin/bulk microphysics treatments, many microphysical processes are represented related to initiation of ice particles and growth of precipitation with dependencies on aerosol chemistry[16,37,38,39,40,41,42,43,44]. The ice crystal and collision-coalescences processes are treated in detail with five microphysical species (cloud-ice crystals, snow, graupel/hail, cloud-droplets and rain) and many chemical species of aerosol particles. Phillips et al.[37] described the relative roles of nucleation processes (homogenous vs. heterogenous processes) in the genesis of cloud particles in the cloud ensemble. SIP is represented via four types of fragmentation including breakup in ice–ice collisions[44], rime splintering[6], fragmentation of freezing rain/drizzle by two modes[16] 1 and 2, and sublimation breakup[45]. AC enables the investigation of the cloud properties and precipitation processes and effect of different environmental conditions on both warm-rain and ice crystal processes.

Two contrasting storms, observed by ground-based and aircraft-based instruments during the STEPS[46] (cloud base is at ~0) and the Midlatitude Continental Convective Clouds Experiment (MC3E[47]; cloud base

is at ~17), were selected for simulations with AC. AC model has already been validated for STEPS case in Phillips et al.[27]. We describe AC and the experimental setup of both cases in the Material and Methods section.

For both multicell mesoscale convective storms (STEPS and MC3E), we tracked the contributions from the warm-rain and ice crystal processes to the precipitation aloft and to the total surface precipitation. Sensitivity tests reveal the influence from various cloud-related environmental conditions, such as aerosol loadings and lower tropospheric moisture governing cloud base, on both processes of precipitation productions.

Results

Results from control simulations:

STEPS—cold-based clouds: control simulation

Hydrometeors profiles associated with warm-rain and ice crystal processes: cold-based clouds

Figure 2 displays the five microphysical species and the warm (red line) and cold (blue line) components of rain and graupel. In the simulated storm, most graupel is from the ice crystal process with riming of snow (Fig. 2e, f). In the STEPS case of cold-based clouds, the abundance of continental aerosol particles (~2500 cm^{-3} at supersaturation of 1% at ~1 km mean sea level (MSL) [27]) makes droplets too small for coalescence (< 20 mean diameter). Both the high CCN concentration and cold cloud base suppress the warm-rain process (red curves in Figs. 2a-d).

The mass and number mixing ratios of cold graupel (blue curves in highlighted regions of Figs. 2a, b) are higher than the corresponding warm components by almost one order of magnitude above freezing level. The simulated ice concentration is highest (~10^5 m^{-3}) at about -40^{o}C (Fig. 2f) in the upper troposphere, due to homogenous freezing. The conditionally averaged number concentration of cloud droplets is just over half an order of magnitude higher near cloud base (~0^{o}C) than at about -30^{o}C (Fig. 2g) due to riming during ascent.

Contribution of warm-rain and ice-crystal processes to surface precipitation: cold-based clouds

Figure 3a shows that by the end of the simulation about 90% of surface precipitation is from the ice crystal process. The warm-rain process is suppressed by the small mean size of cloud droplets from the cold cloud base (~0^{o}C) and continental aerosol conditions (~2500 cm^{-3}), as noted above. At temperatures colder than -10^{o}C, any trace amounts of supercooled "warm-rain" from coalescence can freeze to form "warm graupel", followed by melting as it falls out (Fig. 3a). The cold surface precipitation is from melting of snow and cold graupel. Accumulated stratiform precipitation (Fig. 3c) in this simulated "downburst event"[46] on 19 June is smaller by ~95% compared to convective precipitation (Fig. 3b), because its particles are too small to survive evaporation in the dry deep sub-cloud layer. Overall, cold

precipitation is predicted to dominate both the convective and stratiform components of surface precipitation (upper panel of Fig. S20 (schematic) highlights this result).

MC3E—slightly warm-based clouds: control simulation

Validation of AC

In the second case study, we simulated slightly warm-based deep convective clouds observed during the MC3E campaign on 10-13 May 2011[47]. Among these three days, the MC3E campaign data show that the major convective event was observed on 11 May 2011[47]. AC is evaluated by comparing the observed and modeled cloud properties and aerosol activity. The observed cloud and precipitation features were realistically reproduced, such as the evolution, storm propagation, precipitation rate, radar reflectivity, and vertical velocity statistics of the case. In our case, the predicted cloud parameters show a reasonable agreement with the observations to within the uncertainty limit (Fig. 4).

The simulated and observed CCN spectra (~2000 CCN cm^{-3} at supersaturation of 1% near ground) agree adequately (Fig. 4a). AC also predicts ice nuclei (IN) activity from these aerosol conditions, and this matches nearby IN observations from a similar campaign over the same region and month of another year.

The predicted vertical profiles of concentration (Fig. 4b), diameter (Fig. 4c) of cloud droplets and LWC (Fig. 4d) closely match the observations to within 20-25% at most levels. The predicted ice particle concentrations with their sizes larger than 200(at vertical velocity > 2 ms^{-1}) agrees well with the aircraft observations. We have also validated the predicted ice particle concentrations in the downdraft and stratiform regions. The predicted ice concentration differs from the observations by less than 40% (Fig. 4e). Similarly, predicted and observed vertical profiles of radar reflectivity (Ka-Band ARM Zenith Radars (KAZR)) agree (Fig 4f). Differences between observed and predicted accumulated surface precipitation on 11 May 2011 during 0000-1800 UTC is less than < 10% (Fig. 4g).

Hydrometeors profiles associated with warm-rain and ice crystal processes: slightly warm-based clouds

Above the freezing level, the mass and number mixing ratios of cold graupel are higher and lower by an order of magnitude, respectively, than the corresponding warm components (Fig. 5a, b). Numerous small supercooled drops of rain/drizzle freeze aloft. This contrasts with the cold-based clouds noted above (Fig. 2a, b). Below the freezing level, cold components of mass and number of rain and graupel dominate, but the warm components cannot be ignored (Fig. 5b, d).

Contribution of warm-rain and ice-crystal processes to surface precipitation: slightly warm-based clouds

Figure 6 shows that the warm and cold components of total precipitation accumulated at the ground are comparable throughout this case. The same is true for the convective and stratiform regions. Nearly 60% of the total surface precipitation is from cold precipitation, and the remainder is from the warm-rain process. Overall surface precipitation over the entire domain is mostly from stratiform clouds (>~80%).

As compared to STEPS (Fig. 3), the warm-rain process is more influential due to a warmer cloud base and larger cloud droplets aloft in MC3E (Fig. 6).

In summary, the predicted precipitations at the ground for both convective storms are dominated by the ice-crystal process.

Results from sensitivity simulations:

Sensitivity of warm-rain and ice-crystal processes to cloud base, aerosol conditions, and SIP

To assess the impact from cloud base temperature and CCN loadings on the warm-rain and ice-crystal processes, a sequence of sensitivity tests is done for both STEPS and MC3E. For each of the two cases (STEPS, MC3E), the following perturbation simulations are compared with the corresponding control run:

1. cloud base (CB) is lowered to a warmer level *('Low CB simulation'*),
2. only CCN concentrations are reduced ('*Low CCN simulation*'),
3. both CB height and CCN concentrations are reduced ('*Low CB/CCN simulation*'),
4. IN concentrations are reduced ('*Low IN simulation*'), and
5. all SIP is prohibited ('*no-SIP simulation*')

The low CB simulation involved lowering cloud base without altering the in-cloud ascent statistics (see the Material and Methods section). This isolates the microphysical effects from the warmer temperature of cloud base (e.g., higher adiabatic LWC aloft) in the analysis. Note that in nature, cloud-bases can be lower due to the lower troposphere being either cooler (higher relative humidity) or moister (higher absolute humidity), causing slower or faster in-cloud ascent aloft respectively. There is no simple correspondence between cloud-base height and in-cloud ascent aloft in reality.

In the low CCN and low IN simulations, the loadings of soluble and insoluble solid aerosol species respectively were altered by another height-dependent factor of 0.1 at the ground. This factor was linearly interpolated over height to unity at an altitude of 12 km MSL. This reflects the land-ocean contrast in aerosol loadings[48].

All four types of SIPs were prohibited in the no-SIP simulation. More details of the sensitivity experiments are provided in Material and Method section.

Sensitivity simulations for STEPS

In the low CB sensitivity simulation, the mass and number mixing ratios of "warm graupel" are higher by almost one order of magnitude above freezing level relative to the control simulation (Fig. 7a, b). The other hydrometeor species, such as snow and ice mass, slightly increased in the low CB sensitivity simulation relative to the control simulation (Fig. 7e, f). Above enhancement in the mass mixing ratios of different hydrometeor profiles might affect both the warm and cold components of surface precipitation.

Moreover, in the low CB simulation of STEPS, warming the cloud base, from ~1C in the control run to 18C, augmented the adiabatic LWC and cloud droplet size aloft. This boosted the warm and cold components of surface precipitation by 1000% and 200%, respectively (Fig. 8a) over the entire simulation. Similar changes are found over convective and stratiform regions (Fig. 8b, c). We also use pie charts (Figure 9) to describe fractional contributions of the warm and cold components to the total surface precipitation at the end of the simulation. Figure 9a, b shows that the fractional contribution of the warm-rain process to the total surface precipitation is increased to 54% due to a strengthening of coalescence in low CB run as compared to 20% in the control simulation. This is a remarkable change in the balance between both processes of precipitation, reflecting the paramount importance of cloud base temperature for the microphysical regime of condensate generation. Such a high enhancement of the warm component of surface precipitation is due to the faster rates of collision and coalescence of larger cloud droplets aloft when the adiabatic LWC is boosted by more moisture in the PBL. The moistened PBL intensifies raindrop freezing aloft, producing more warm graupel and enhancing the warm precipitation at the surface. The lower cloud base also slightly promotes cold surface precipitation—yet less so than its strong boost of warm surface precipitation—from the ice crystal process because more supercooled cloud liquid (Fig. S6) intensifies riming of snow and graupel.

In low CCN simulation, Fig. 9b, c shows that the fractional contribution of the warm components to the total surface precipitation is slightly increased to 23% at most in-cloud levels compared to 20% in control. The absolute amounts of the warm and cold components of total surface precipitation in the low CCN simulation are moderately changed by the end of the simulation relative to the control run (Fig. 8d-f). These changes in the warm and cold components of total surface precipitation are minimal because the STEPS control simulation involves little activity of the CCN-sensitive warm-rain process as cloud droplets were too small to coalesce[27]. Fewer CCN can reduce the aerosol-induced invigoration of convection, reducing the supply of moisture for conversion to precipitation[49]. This reduction of CCN loadings can also lower the level of warm-rain during ascent with less evaporation during shorter fallout to the ground (solid red line in Fig. 8d), causing a slight increase in the warm-rain process led to total surface precipitation.

In the low CB/CCN simulation, Fig. 8g shows that the absolute contribution from the warm (cold) component to the total surface precipitation is more than 1300% (130%) higher at the end of the simulation than the corresponding control run. The total surface precipitation increased by more than a factor of 4 beyond the control run. Fig. 9b, d shows that the fractional contribution of the warm-rain process to the total surface precipitation is increased to 65% compared to 20% in the control. The fractional contribution from the ice-crystal process is reduced to 35% from 80%. The maximum of the average number concentrations of cloud droplets is reduced by one order of magnitude when compared to that of the control run (Fig. S12g). Also, the average diameter of cloud droplets was doubled (an increase by ~8-10) (Fig. S6a). These larger cloud droplets coalesce more efficiently to form rain[22], which may freeze if supercooled, strongly augmenting the warm components of total surface precipitation. The strengthening of raindrop freezing in the mixed-phase region (0 to -36C) and the melting and freezing of

warm graupel could also increase the warm component of surface precipitation. This is consistent with the alteration of ice multiplication by warm graupel (Fig. S12f). Above results explain why the low CB/CCN simulation produces more warm components of the total surface precipitation.

In the low IN simulation, Figure 8j shows that the warm and cold components of total surface precipitation are relatively less sensitive to the reduction of active IN concentrations than the control run. The fractional contribution of the warm components to total surface precipitation is increased to 19.9% from 19.5% than the control run (Fig. 9b, e). The slight increase in the warm components in the low IN simulation could be because the fewer active IN enhance the concentrations of supercooled cloud droplets, thereby increasing the riming and freezing of raindrops, increasing the warm graupel and warm components of surface precipitation. Ice multiplication causes the average number concentration of crystals to be almost unchanged in this sensitivity test (Fig. S13f), as also explained by Phillips et al[27].

In the no-SIP simulation, the fractional contribution of the warm component to total surface precipitation is increased to 25% from 20% in the control run (Fig. 9b, f). The absolute increase in warm and cold components is, respectively, 300% and 350% (Fig. 8m). The total surface precipitation in the no-SIP simulation is increased by a factor of 2 beyond the control run (Fig. 8m). In the no-SIP simulation, the increased average size of cloud ice crystals (and decrease in ice-crystal number concentrations) intensify the overall cold precipitation and thereby total surface precipitation compared to the control run (Fig. S6b). Larger crystals grow by aggregation and vapor deposition to form snow more rapidly. Overall, the no-SIP simulation showed little effect on the average size and number concentrations of cloud droplets (Fig. S6a, c). Thus, the increase in the warm component of total surface precipitation in the no-SIP simulation is primarily associated with the strengthening of the collisional raindrop freezing from the larger ice crystals and more formation of warm graupel.

Sensitivity simulations for MC3E

In the low CB simulation, lowering cloud base by warming it by ~11K (from ~17 in the control) affects the warm components of total surface precipitation more strongly than the cold components. Figure 10a shows the absolute contribution from the warm (cold) component to the total surface precipitation is increased in low CB simulation by about 170% (35%) relative to the corresponding control run at the end of the simulation. Moreover, the fractional contribution of the warm-rain process to the total surface precipitation is increased to 42% from 24% in the control simulation (Fig. 11a, b). This is because of the lowering of cloud base involves moistening of the lower troposphere which yields a greater mass of condensate from condensation for coalescence to form precipitation. In this low CB simulation, the mass mixing ratio of rain (particularly warm component) intensifies below freezing level, yielding more warm precipitation at the surface (Fig. S15c). As stated above, the moistened PBL intensifies raindrop freezing aloft and increases the warm graupel mass. This in turn also contributes to the enhancement of the warm precipitation at the surface. Qualitatively, the manner of this response to lowering cloud base is similar to that noted above for STEPS case.

In the low CCN simulation, Figure 11b, c shows that the fractional contribution of the warm component to the total surface precipitation is increased to 29% at most in-cloud levels compared to 24% in control run. By the end of the simulation, the absolute contributions from the warm and cold components show an increase by ~10% and a decrease by ~10% relative to the control run respectively, causing little change in the total surface precipitation due to this compensation (Fig. 10d). In this low CCN simulation, the increase in cloud droplet size by more than 30% throughout the vertical column relative to the control run causes an enhancement in the warm component of total surface precipitation (Fig. S8a). However, the mean size of ice crystals is slightly reduced in the mixed-phase region (Fig. S8b), causing the reduction of the cold contributions to the total surface precipitation.

In the low CB/CCN simulation, there is almost the strongest response out of all the sensitivity tests presented here because now the lowering of both cloud base and CCN concentrations act in concert in the same direction, enhancing coalescence. The fractional contribution of the warm-rain process to the total surface precipitation is increased to 49%, due to a strengthening of coalescence at most in-cloud levels, compared to 24% in control (Fig. 11b, d). The fractional contribution from the ice-crystal process is reduced to 51% from 76%. The absolute increase in warm (cold) components of total surface precipitation is more than 250% (58%) at the end of the simulation relative to the control run. The total surface precipitation increased by nearly a factor of 2 beyond the control run. Interestingly, over convective regions, the fractional contribution of warm components to the surface precipitation is increased to 82% from 41% (Fig. 12b, d). This increase in the low CB/CCN simulation is noted to be greatest relative to the control run. The average diameter of cloud droplets was increased by ~33% in the lower to middle troposphere relative to the control run (Fig. S8a). As compared to the control run, the higher growth of average diameter of cloud droplets and reduced adiabatic LWC (by almost 66%) can enhance the coalescence efficiency and hence the warm components of total surface precipitation. The partial increase in the cold components of total surface precipitation relative to control run is due to enhanced growth of ice crystal diameter and reduced ice water content (IWC) below -30 (Fig. S8d).

In the low IN simulation, Figure 10j-l shows that the warm and cold components of total surface precipitation are relatively less sensitive to the lowering of ice nuclei than the control run. This lack of response is similar to that found with the STEPS case noted above.

In the no-SIP simulation, at the end of the simulation, the absolute increase in warm components is 130% more than the control run (Fig. 10m), whereas the absolute decrease in cold components is 40%. The fractional contribution of the warm components to total surface precipitation arises to 52% from 24% than the control run (Fig. 11b, f). The no-SIP simulation showed a relatively stronger effect on the cloud droplet size and cloud droplets number concentrations than the control run, which contrasts with the STEPS case. The increase in the warm components of total surface precipitation in the no-SIP simulation is associated with the strengthening of both the ice crystal size and cloud droplet sizes above -25 (Fig. S8a, b). The increase ice cloud fraction by 100% relative to the control show that the increase in ice-cloud lifetime and the lesser cold precipitation (Fig. S10b).

In summary, among all the MC3E sensitivity tests, the greater increase in the fractional contribution from warm components to the total precipitation is mainly associated with the low CB and no-SIP simulations relative to the control run. This indicates the strong sensitivity of warm components of liquid and ice precipitation with respect to the cloud base temperature and multiple mechanisms of ice multiplication.

Discussion And Conclusions

The present study assesses how the warm-rain and ice-crystal (cold rain) processes drive surface precipitation for two different observed convective storms—STEPS (cold-based convective clouds) and MC3E (slightly warm-based convective clouds) using AC.

The conclusions are as follows:

1. The ice crystal process prevails in the cloud properties aloft for the control simulations of both cases of deep convection, even though one of them is slightly warm-based (MC3E):

    a. In STEPS and MC3E, the cold components of precipitation aloft are more prominent by almost one and two orders of magnitude, respectively, relative to the corresponding warm components, for both mass and number mixing ratios of graupel and rain.

    b. With STEPS, the cold cloud base (~1) suppresses the warm-rain process due to the low adiabatic LWC from the dry lower troposphere, slightly assisted also by the higher normalized CCN concentration (~2500 cm^{-3} at supersaturation of 1% at ~1 km MSL; Phillips et al.[27]). The lack of moisture makes cloud droplets too small to coalesce (20).

    c. In MC3E, both precipitation processes are stronger than in STEPS due to the greater adiabatic LWC. The ice crystal process is strengthened by the long-lived stratiform clouds from convective outflows. Again, the warm-rain process is impeded by the smallness of cloud droplets (<17) at all levels and never prevails.

2. By the end of both control simulations of STEPS and MC3E, about 80% of accumulated surface precipitation over the entire mesoscale domain is dominated by the ice-crystal process. Only 20% is from the warm-rain process. A similar predominance of the ice-crystal process happens in each of the convective and stratiform regions. Stratiform and convective regions prevail in surface precipitation in the MC3E and STEPS cases, respectively.
3. All sensitivity tests reveal a tendency for both types of precipitation to compete, such that one increases at the expanse of the other, in absolute amounts of surface precipitation. Specifically, sensitivity tests with both validated AC simulations show the following influences:

    a. In both cases, the lowering of cloud base to the warmer levels near the ground ('Low CB simulation'), by 18K in STEPS and 11K in MC3E, causes an increase in the fractional and absolute contributions from the warm components of surface precipitation. This reflects the moistening of the lower tropospheric environment, promoting condensational growth of cloud droplets aloft. They attain the critical size for coalescence sooner during ascent. Overall, we see

that the warm components comprise about half of the total surface precipitation in both low CB runs. The mean cloud droplet size, ice crystal size, LWC, IWC, and cloud cover all exhibit stronger increases (> ~10-30%) at subzero levels in STEPS than MC3E (mostly decreases by ~10-20%) when cloud base is lowered.

b. The reduction in CCN and IN concentrations (low CCN and low IN simulations) towards maritime aerosol conditions only weakly enhances (< 10%) the fractional and absolute contributions of warm components to the surface precipitation. This occurs over the entire mesoscale domain and over convective and stratiform regions individually.

c. In both cases, when both cloud base (CB) height and CCN concentrations are reduced ('*Low CB/CCN simulation*') together, the greatest increase in fractional contributions from warm components to the surface precipitation was by 53% (from about 20% in control to ~73%) over stratiform regions in STEPS and similarly over convective regions in MC3E.

d. When all four mechanisms of SIP are switched off ('no-SIP simulation'), the absolute change in surface precipitation is an increase of ~110% in STEPS and ~25% in MC3E case at the end of the simulation. The fractional contribution from warm components to the surface precipitation over the entire mesoscale domain is enhanced by almost 30% (from about 24% in control to 54%) in MC3E. This suggests a strong sensitivity of warm components of rain and graupel/hail with respect to the multiple mechanisms of ice multiplication in slightly warm-based convective clouds. The corresponding change in STEPS is only 6% (from about 19% in control to 25%) due to the weaker warm-rain process. Note that in the real atmosphere, secondary ice production is always present in deep cold precipitating clouds. The purpose of this idealized test was to analyze causation in the control simulations.

Some of our detailed simulations, such as those with low cloud base and maritime CCN concentrations, show that surface precipitation and graupel/hail aloft can be dominated by the warm-rain process, even though there is plenty of ice aloft. This happens due to raindrop freezing (from the warm-rain process) almost instantly generating graupel, circumventing the lengthy vapor growth of crystals to snow and then by riming to graupel (ice-crystal process). This is consistent with earlier modeling[50,15]. Also, coalescence occurs earlier and closer to the ground during deep cloudy ascent while crystals only appear later at subzero levels.

The assumption is made in some satellite-based and global modeling studies that surface precipitation is cold merely because ice is present somewhere aloft in the cloudy column[19,20]. Our simulations prove that such an assumption is not universally valid because ice is always present aloft even when warm rain prevails at the surface (low CB and low CB/CCN simulations in STEPS and MC3E). Also, there is no theoretical basis in cloud microphysics for such an assumption.

Identification of warm and cold components of surface precipitation, and the role of various physical processes in influencing them, is important for reducing the uncertainties in global climate models. Our simulations presented here indicate a central role of raindrop freezing as a source of precipitation

associated with the warm-rain process: warm-graupel is uniquely efficient at accreting liquid as it falls fast and has a wide cross-sectional area from a low bulk density.

This study pioneers how to use passive tagging tracer techniques so as to determine the competition between warm-rain and ice-crystal processes in the genesis of surface precipitation. The inclusion of passive tagging tracers techniques in the global climate model could be useful in predicting these warm and cold types of surface precipitation.

Declarations

Acknowledgments:

This work was completed for a past award to VTJP from the Crafoord Foundation (award number: 20180783) supporting the first author during his postdoc tenure at LU, Sweden. The work was planned and directed by VTJP. Other authors were supported by two research grants to VTJP, from the Swedish Research Council for Sustainable Development (“FORMAS” Award 2018-01795) and the U.S. Department of Energy Atmospheric SciencesResearch Program (Award DE-SC0018932). The topics ofthese awards concern mechanisms for ice production in clouds.

Funding:

VTJP obtained the funding from the Crafoord Foundation (award number: 20180783) to support first author. Other authors were supported by the Swedish Research Council for Sustainable Development (“FORMAS” Award 2018-01795) and the U.S. Department of Energy Atmospheric SciencesResearch Program (Award DE-SC0018932).

Author contributions:

VTJP contributed to conceptual development of this work. AG developed the passive tagging tracers codes with VTJP for tracking the warm-rain and ice crystal processes driven precipitation. AG drafted the original manuscript. The manuscript was edited by VTJP, SP, DW and reviewed by AB, AD and AY.

Data and materials availability:

The MC3E ground-based (and aircraft-based) data for simulation is available in public domain and it can be obtained from https://ghrc.nsstc.nasa.gov/hydro/details/gpmcmmc3e. The STEPS sounding data can be obtained from https://data.eol.ucar.edu/project/STEPS. Underlying data related to main manuscript (including supplementary figures data) generated using AC will be available at the time of publication or before first revision.

Competing interests:

Authors declare that they have no competing interests.

Code availability:

The code that was used for the analysis and generating figures will also be available at the time of publication or before first revision. The primary AC model is based on WRF4 (https://github.com/wrf-model/WRF/releases) with various modifications in microphysics scheme developed over many years by Phillips et al[15,16,37,38,39,40,41,42,43,44].

References

1. Sherwood, S. C. et al. An assessment of Earth's climate sensitivity using multiple lines of evidence. *Rev. of Geophys.* 58, e2019RG000678 (2020).
2. O'Gorman, P. A. Precipitation extremes under climate change. Current climate change reports, *1*(2), 49–59 (2015).
3. Zhang, Y. & Fueglistaler, S. Mechanism for increasing tropical rainfall unevenness with global warming. Geophys. Res. Lett., 46(24), 14836–14843 (2019).
4. Warner, J. A. reduction in rainfall associated with smoke from sugar-cane fires—an inadvertent weather modification? J. Appl. Meteorol. and Climatol., *7*(2), 247–251 (1968).
5. Liu, J. Y., & Orville, H. D. Numerical modeling of precipitation and cloud shadow effects on mountain-induced cumuli. J. Atmos. Sci., *26*(6), 1283–1298 (1969).
6. Hallett, J. & Mossop, S. C. Production of secondary ice particles during the riming process. Nat., 249, 26–28 (1974), doi:10.1038/ 249026a0.
7. Twomey, S. The nuclei of natural cloud formation part I: The chemical diffusion method and its application to atmospheric nuclei. Geofisica pura e applicata, *43*(1), 227–242 (1959).
8. Albrecht, B. A. Aerosols, cloud microphysics, and fractional cloudiness. Science, *245*(4923), 1227–1230 (1989).
9. Williams, E. & Stanfill, S. The physical origin of the land–ocean contrast in lightning activity. Comptes Rendus Physique, *3*(10), 1277–1292 (2002).
10. Khain, A., Pokrovsky, M. P., Seifert, A., & Phillips, V. T. J. Simulation of effects of atmospheric aerosols on deep turbulent convective clouds using a spectral microphysics mixed-phase cumulus cloud model. Part I: Model description and possible applications. J. Atmos. Sci., 61, 2963–2982 (2004).
11. Williams, E. et al. The drought of the century in the Amazon Basin: An analysis of the regional variation of rainfall in South America in 1926. Acta Amazonica, *35*(2), 231–238 (2005).
12. Bringi, V. N. et al. Evolution of a Florida thunderstorm during the Convection and Precipitation/Electrification Experiment: The case of 9 August 1991. Mon. Weather Rev., *125*(9), 2131–2160 (1997).
13. Hallett, J., Sax, R. I., Lamb, D., & Murty, A. S. R. Aircraft measurements of ice in Florida cumuli. Q. J. R. Meteorol. Soc., 104: 631–651 (1978).

14. Phillips, V. T. J. et al. The glaciation of a cumulus cloud over New Mexico. Quart. J. Roy. Meteor. Soc., 127, 1513–1534 (2001).
15. Phillips, V. T. J., Choularton, T. W., Blyth, A. M. & Latham, J. The influence of aerosol concentrations on the glaciation and precipitation production of a cumulus cloud. Quart. J. Roy. Meteor. Soc., 128, 951–971 (2002).
16. Phillips, V. T. J., Patade, S., Gutierrez, J., & Bansemer, A. Secondary ice production by fragmentation of freezing drops: Formulation and theory. J. Atmos. Sci., 75(9), 3031–3070 (2018).
17. Johnson, D. B. On the relative efficiency of coalescence and riming. J. Atmos. Sci, **44**, 1671–1680 (1987).
18. Phillips, V. T. J. et al. Anvil glaciation in a deep cumulus updraught over Florida simulated with the explicit microphysics model. I: Impact of various nucleation processes. Quart. J. Roy. Meteor. Soc., 131, 2019–2046 (2005).
19. Mülmenstädt, J., Sourdeval, O., Delanoë, J., & Quaas, J. Frequency of occurrence of rain from liquid-, mixed-, and ice-phase clouds derived from A-Train satellite retrievals. Geophys. Res. Lett., *42*(15), 6502–6509 (2015).
20. Field, P. R., and A. J. Heymsfield. Importance of snow to global precipitation. Geophys. Res. Lett. 42(21): 9512–9520 (2015).
21. Houghton, H. G. A preliminary quantitative analysis of precipitation mechanisms. J. Atmos. Sci. 7(6), 363–369 (1950).
22. Rogers, R. R., & M. K. Yau. A short course of cloud physics. Pregamon. (1989).
23. Fan, J., Zhang, R., Li, G. & Tao, W.K. Effects of aerosols and relative humidity on cumulus clouds. J. Geophys. Res. Atmos., *112*(D14) (2007).
24. Field, P. R. et al. Exploring the convective grey zone with regional simulations of a cold air outbreak. Q. J. Royal Meteorol. Soc., *143*(707), 2537–2555 (2017).
25. Harris-Hobbs, R. L. & Cooper, W. A. Field evidence supporting quantitative predictions of secondary ice production rates. J. Atmos. Sci., *44*(7), 1071–1082 (1987).
26. Blyth, A. M. & Latham, J. Development of ice and precipitation in New Mexican summertime cumulus clouds. Q. J. Roy. Meteorol. Soc., 119: 91–120 (1993).
27. Phillips, V. T. J. et al. Ice multiplication by breakup in ice–ice collisions. Part II: Numerical simulations. J. Atmos. Sci., 74, 2789–2811 (2017b).
28. Koenig, L. R. The glaciating behavior of small cumulonimbus clouds. J. Atmos. Sci., *20*(1), 29–47 (1963).
29. Blyth, A. M., Benestad, R. E., & Krehbiel, P. R. Observations of supercooled raindrops in new Mexico Summertime Cumuli. J. Atmos. Sci., 54, 569–575 (1997).
30. Patade, S., Shete, S., Malap, N., Kulkarni, G., & Prabha, T. V. Observational and simulated cloud microphysical features of rain formation in the mixed phase clouds observed during CAIPEEX. Atmos. Res., *169*, 32–45 (2016).

31. Morrison, H.C., Curry, J. A. & Khvorostyanov, V. I. A new double-moment microphysics parameterization for application in cloud and climate models. Part I: Description. J. Atmos. Sci., *62*(6), 1665–1677 (2005).
32. Morrison, H., Thompson, G. & Tatarskii, V. Impact of cloud microphysics on the development of trailing stratiform precipitation in a simulated squall line: Comparison of one-and two-moment schemes. Mon. Weather Rev., *137*(3), 991–1007 (2009).
33. Lin, Y., & Colle, B. A. The 4–5 December 2001 IMPROVE-2 event: Observed microphysics and comparisons with the Weather Research and Forecasting model. Mon. Weather Rev., *137*(4), 1372–1392 (2009).
34. Khain, A. P., Phillips, V. T. J., Benmoshe, N., & Pokrovsky, A. The role of small soluble aerosols in the microphysics of deep maritime clouds. J. Atmos. Sci., *69*(9), 2787–2807 (2012).
35. Milbrandt, J. A., & Yau, M. K. A multimoment bulk microphysics parameterization. Part I: Analysis of the role of the spectral shape parameter. J. Atmos. Sci., *62*(9), 3051–3064 (2005a).
36. Milbrandt, J. A., & Yau, M. K. A multimoment bulk microphysics parameterization. Part II: A proposed three-moment closure and scheme description. J. Atmos. Sci., *62*(9), 3065–3081 (2005b).
37. Phillips, V. T. J., Donner, L. J. & Garner. S. T. Nucleation processes in deep convection simulated by a cloud-system-resolving model with double-moment bulk microphysics. J. Atmos. Sci., 64(3) 738–761 (2007).
38. Phillips, V. T. J. et. al. Multiple environmental influences on the lightning of cold-based continental cumulonimbus clouds. Part I: Description and validation of model. J. Atmos. Sci., 77(12), 3999–4024 (2020).
39. Phillips, V. T. J., DeMott, P. J., & Andronache, C. An empirical parameterization of heterogeneous ice nucleation for multiple chemical species of aerosol. J. Atmos. Sci., 65, 2757–2783 (2008).
40. Phillips, V. T. J. et al. Potential impacts from biological aerosols on ensembles of continental clouds simulated numerically. Biogeosciences, *6*(6), 987–1014 (2009).
41. Phillips, V. T. J. et al. Improvements to an empirical parameterization of heterogeneous ice nucleation and its comparison with observations. J. Atmos. Sci., 70, 378–409 (2013).
42. Phillips, V. T. J., Khain, A., Benmoshe, N., & Ilotoviz, E. Theory of time-dependent freezing. Part I: Description of scheme for wet growth of hail. J. Atmos. Sci., *71*(12), 4527–4557 (2014).
43. Phillips, V. T. J., Khain, A., Benmoshe, N., Ilotoviz, E., & Ryzhkov, A. Theory of time-dependent freezing. Part II: Scheme for freezing raindrops and simulations by a cloud model with spectral bin microphysics. J. Atmos. Sci., *72*(1), 262–286 (2015).
44. Phillips, V. T. J., Yano, J. I., & Khain, A. (2017a). Ice multiplication by breakup in ice–ice collisions. Part I: Theoretical formulation. J. Atmos. Sci., *74*(6), 1705–1719.
45. Deshmukh, A., Phillips, V. T. J., Bansemer, A., Patade, S., & Waman, D. New Empirical Formulation for the Sublimational Breakup of Graupel and Dendritic Snow. J. Atmos. Sci., *79*(1), 317–336 (2022).

46. Lang, T. J. et al. The severe thunderstorm electrification and precipitation study. Bull. Am. Meteorol. Soc., *85*(8), 1107–1126 (2004).
47. Jensen, M. P. et al. The Midlatitude Continental Convective Clouds Experiment (MC3E), Bull. Am. Meteorol. Soc., 97, 1667–1686 (2016).
48. Pruppacher, H. R., & Klett, J. D. *Microphysics of Clouds and Precipitation*. *2d ed. Oxford Press*, 953 (1997).
49. Li, G., Wang, Y., Lee, K. H., Diao, Y., & Zhang, R. Impacts of aerosols on the development and precipitation of a mesoscale squall line. J. Geophys. Res. Atmos., *114*(D17) (2009).
50. Chisnell, R. F., & Latham, J. Multiplication of Ice Particles in Slightly Supercooled Cumulus, J. Atmos. Sci., *32*(4), 863–866 (1975).
51. Tian, J., Dong, X., Xi, B., Williams, C. R., & Wu, P. Estimation of liquid water path below the melting layer in stratiform precipitation systems using radar measurements during MC3E. Atmos. Measurement Techn., *12*(7), 3743–3759 (2019).
52. Phillips, V. T. J. Ice multiplication by fragmentation during quasi-spherical freezing of raindrops: A theoretical investigation. J. Atmos. Sci., *78*(10), 3215–3228 (2021).
53. Heymsfield, A. J. Precipitation development in stratiform ice clouds: A microphysical and dynamical study. J. Atmos. Sci., *34*(2), 367–381 (1977).
54. Heymsfield, A. J. et al. Observations and parameterizations of particle size distributions in deep tropical cirrus and stratiform precipitating clouds: Results from in situ observations in TRMM field campaigns. J. Atmos. Sci., *59*(24), 3457–3491 (2002).
55. Zhang, Q. et al. Spatial and temporal variability of precipitation maxima during 1960–2005 in the Yangtze River basin and possible association with large-scale circulation. J. Hydrolo., *353*(3–4), 215–227 (2008).
56. Hong, S. Y., Dudhia, J., & Chen, S. H. A revised approach to ice microphysical processes for the bulk parameterization of clouds and precipitation. Mon. Weather Rev., *132*(1), 103–120 (2004).
57. Ulbrich, C. W. Natural variations in the analytical form of the raindrop size distribution. J. clim. Appl. Meteorol., 1764–1775 (1983).
58. Ulbrich, C. W. The effects of drop size distribution truncation on rainfall integral parameters and empirical relations. J. Appl. Meteorol. Climatol., *24*(6), 580–590 (1985).
59. Kozu, T., & Nakamura, K. Rainfall parameter estimation from dual-radar measurements combining reflectivity profile and path-integrated attenuation. J. Atmos. Oceanic Tech., *8*(2), 259–270 (1991).
60. Rose, C. R., & Chandrasekar, V. A GPM dual-frequency retrieval algorithm: DSD profile-optimization method. J. Atmos. Oceanic Tech., *23*(10), 1372–1383 (2006).
61. McFarquhar, G. M., & Heymsfield, A. J. Parameterization of tropical cirrus ice crystal size distributions and implications for radiative transfer: Results from CEPEX. J. Atmos. Sci., *54*(17), 2187–2200 (1997).

62. Heymsfield, A. J., Bansemer, A., Schmitt, C., Twohy, C., & Poellot, M. R. Effective Ice Particle Densities Derived from Aircraft Data, J. Atmos. Sci., *61*(9), 982–1003 (2004).
63. Tripoli, G. J., & Cotton, W. R. A numerical investigation of several factors contributing to the observed variable intensity of deep convection over south Florida. J. Appl. Meteorol. Climatol., *19*(9), 1037–1063 (1980).
64. Khairoutdinov, M., & Kogan, Y. A new cloud physics parameterization in a large-eddy simulation model of marine stratocumulus. Monthly weather review, *128*(1), 229–243 (2000).
65. Pawlowska, H., & Brenguier, J. L. An observational study of drizzle formation in stratocumulus clouds for general circulation model (GCM) parameterizations. Journal of Geophysical Research: Atmospheres, *108*(D15) (2003).
66. Seifert, A. & Beheng, K. D. A two-moment cloud microphysics parameterization for mixed-phase clouds. Part 1: Model description. Meteor. Atmos. Phys., 92, 45–66 (2005).
67. Kogan, Y. A cumulus cloud microphysics parameterization for cloud-resolving models. J. Atmos. Sci., *70*(5), 1423–1436 (2013).
68. Phillips, V. T. J., Illingworth, A. J., Hogan, R. J., & Field. P. R. Simulations of the glaciation of a frontal mixed-phase cloud with the explicit microphysics model (EMM). Q. J. Roy. Meteor. Soc., 129, 1351–1371 (2003).
69. Phillips, V. T. J., & Patade, S. Multiple Environmental Influences on the Lightning of Cold-Based Continental Convection. Part II: Sensitivity Tests for Its Charge Structure and Land–Ocean Contrast, J. Atmos. Sci., *79*(1), 263–300 (2022).
70. Williams, E., & Stanfill, S. The physical origin of the land–ocean contrast in lightning activity. Comptes Rendus Physique, *3*(10), 1277–1292 (2002).

Figures

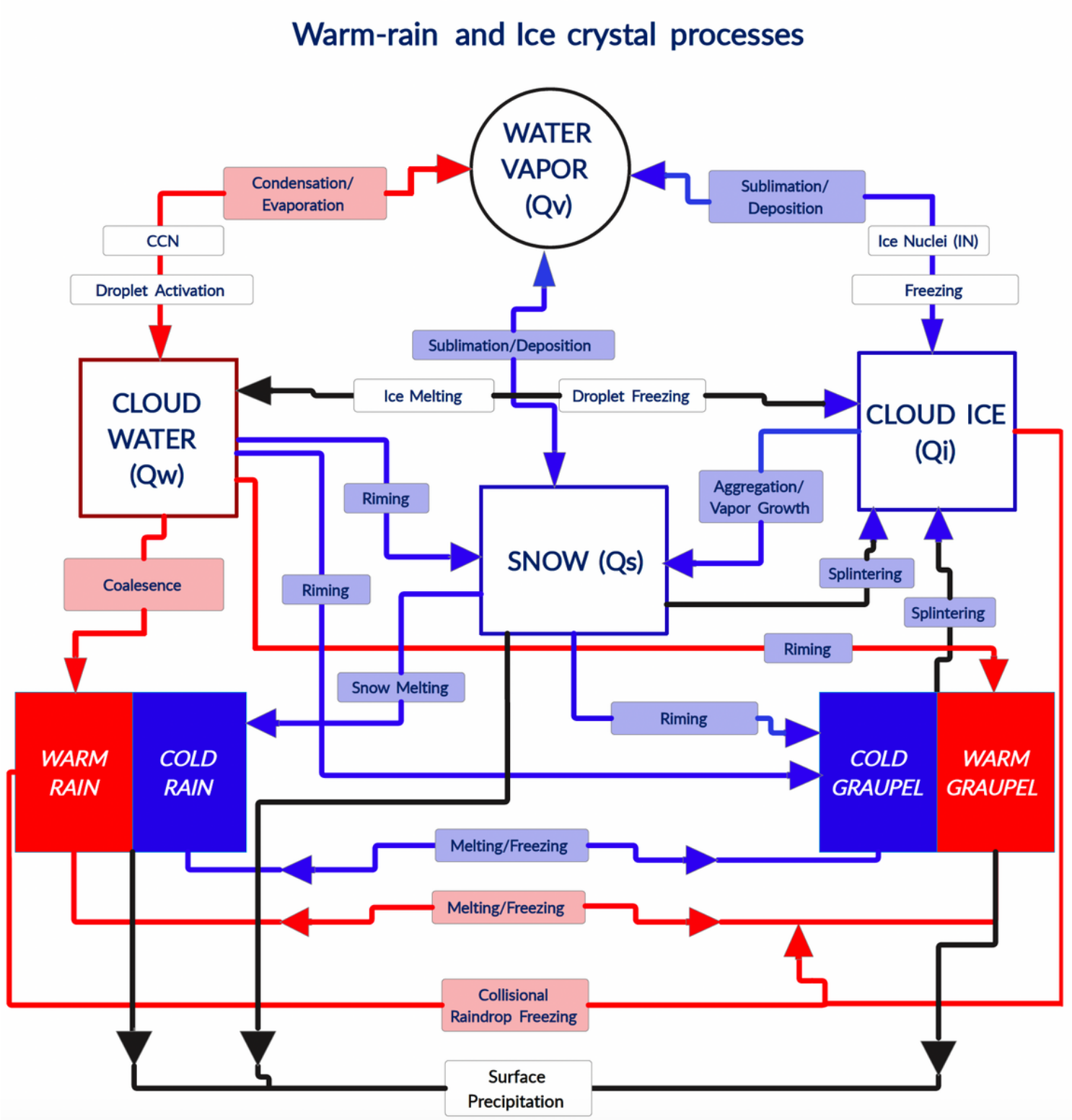

Figure 1

Schematic diagram representing the web of cloud microphysical processes involving warm-rain and ice crystal processes. The red color of lines and arrows denotes the warm-rain process, and their blue color highlights the ice crystal process. The black color denotes the conversions that could be part of either process.

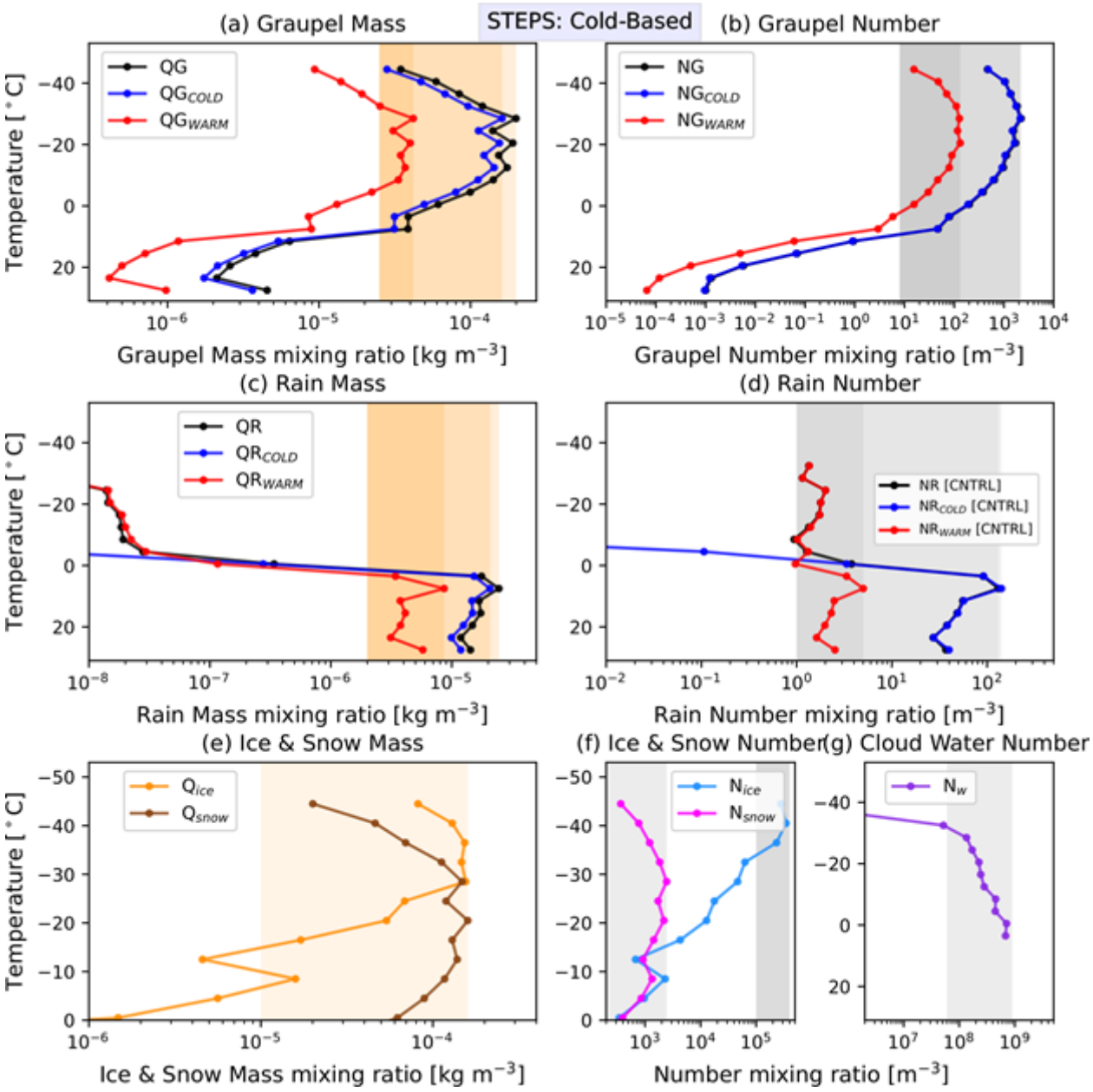

Figure 2

Temperature-resolved conditionally averaged over cloudy regions of: (a)-(b) mass and number mixing ratios of graupel with corresponding warm (red line) and cold (blue line) components; (c)-(d) mass and number mixing ratios of rain plotted similarly; (e) ice and snow mass mixing ratio; (f) ice and snow number mixing ratio; and (g) cloud water number mixing ratio for the STEPS case (cold-based convective clouds at ~0) control simulation using AC during 2345 UTC 19 June–0215 UTC 20 June 2000 (except without first hour of simulation).

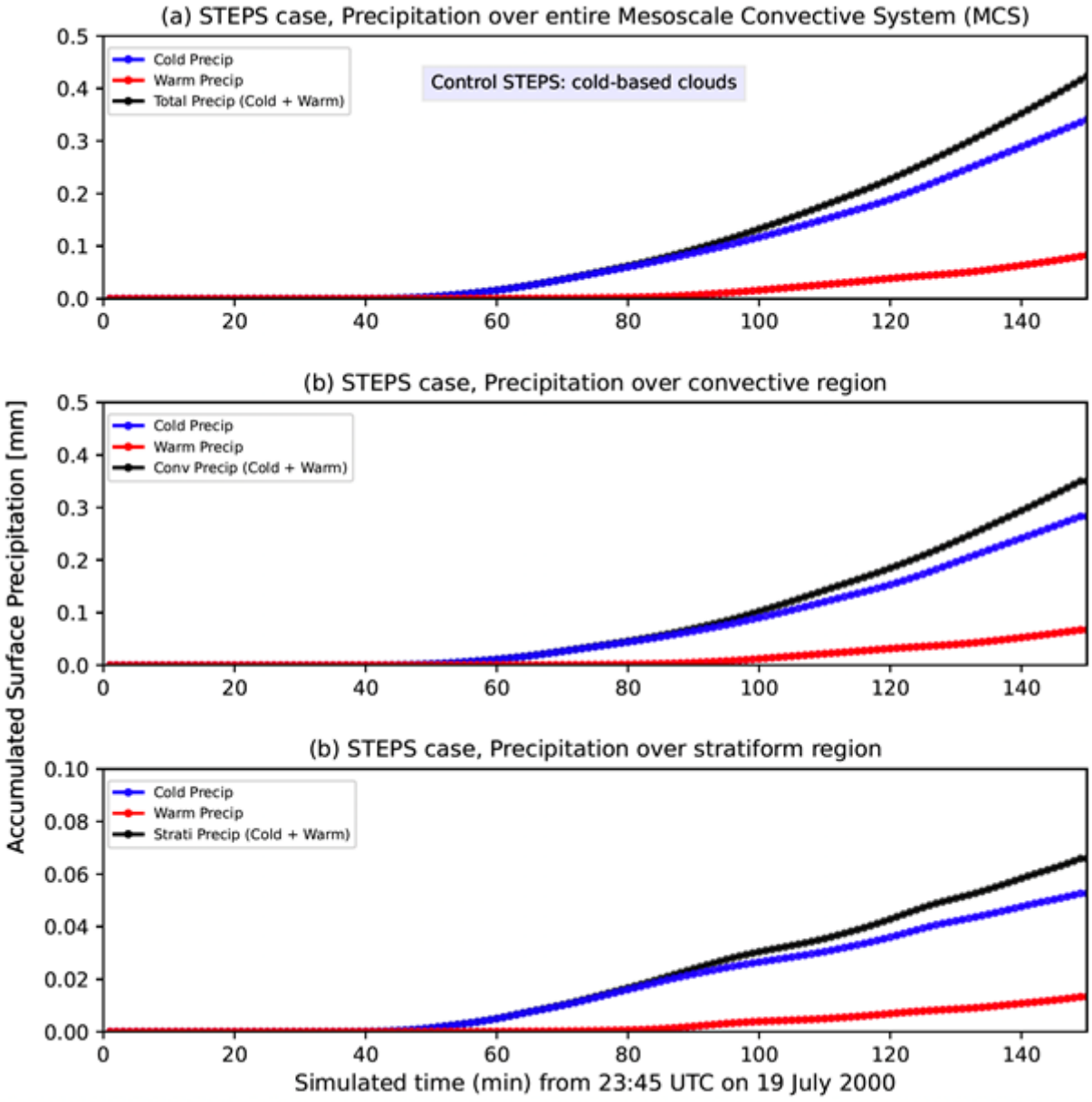

Figure 3

STEPS case control simulation of the accumulated precipitation (mm) under (a) total cloudy condition, (b) convective, (c) stratiform during 2345 UTC 19 Jun–0215 UTC 20 Jun 2000.

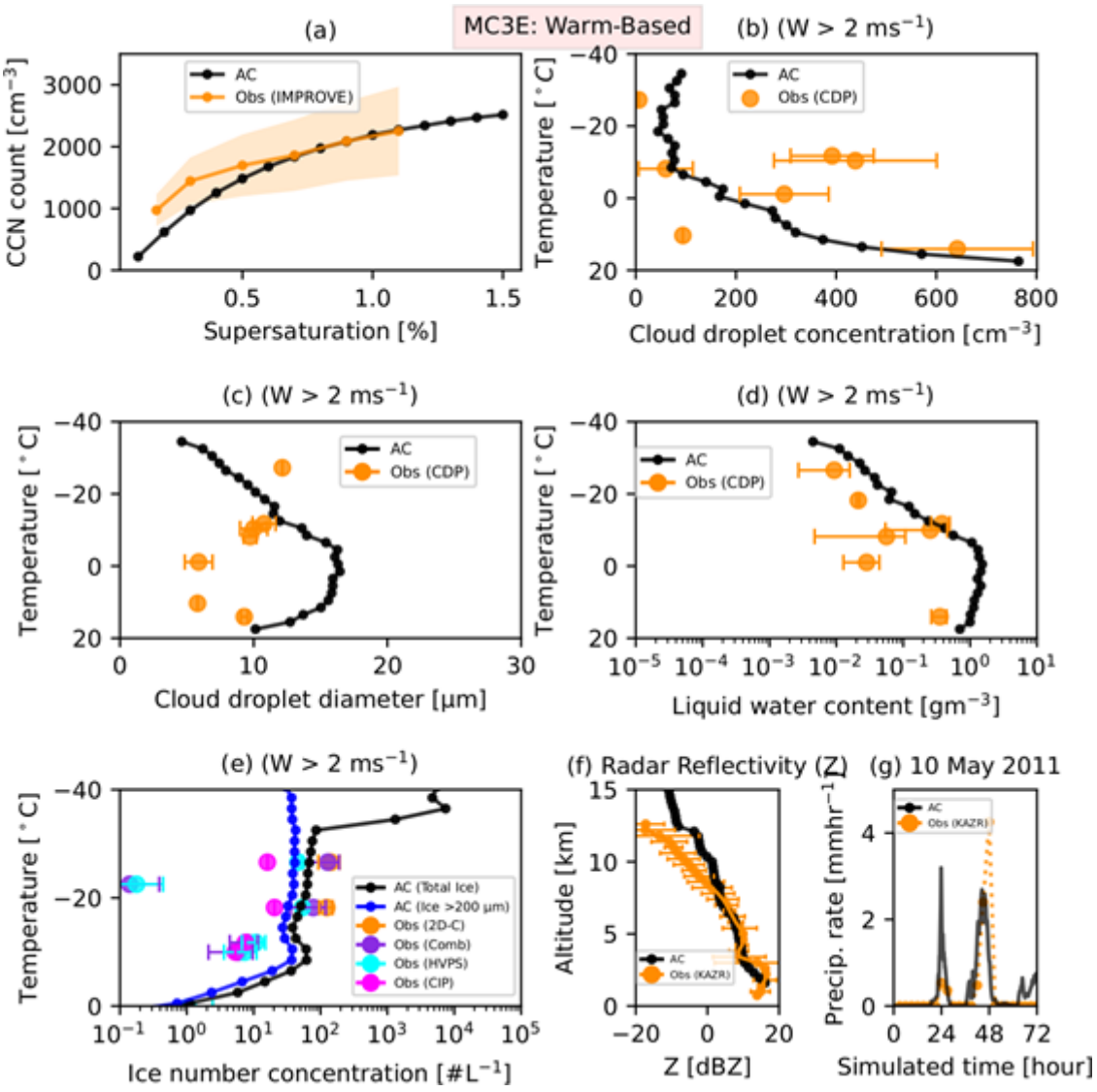

Figure 4

Comparison of AC control simulations of the MC3E case with the radar and ground-based observations for (a) the CCN activity spectra (yellow shaded region indicates uncertainty related to measurement); (b) number concentration of cloud droplets, (c) cloud drop diameter, and (d) liquid water content, with vertical velocity > 2 ms^{-1}; (e) ice number concentration with vertical velocity > 2 ms^{-1}; (f) radar reflectivity and (g) precipitation rate. CCN observations were taken using CCN-100 counter deployed at Lamont, Oklahoma. Aircraft-based observations from 2D-C, cloud imaging probe (CIP), High Volume Precipitation Spectrometer-3 (HVPS-3) probe, and the combined data from these probes (COMB) are used for the validation of ice number concentration with AC model. Aircraft-based cloud droplet probe (CDP) observations are used for validation of cloud droplet size and number concentration.

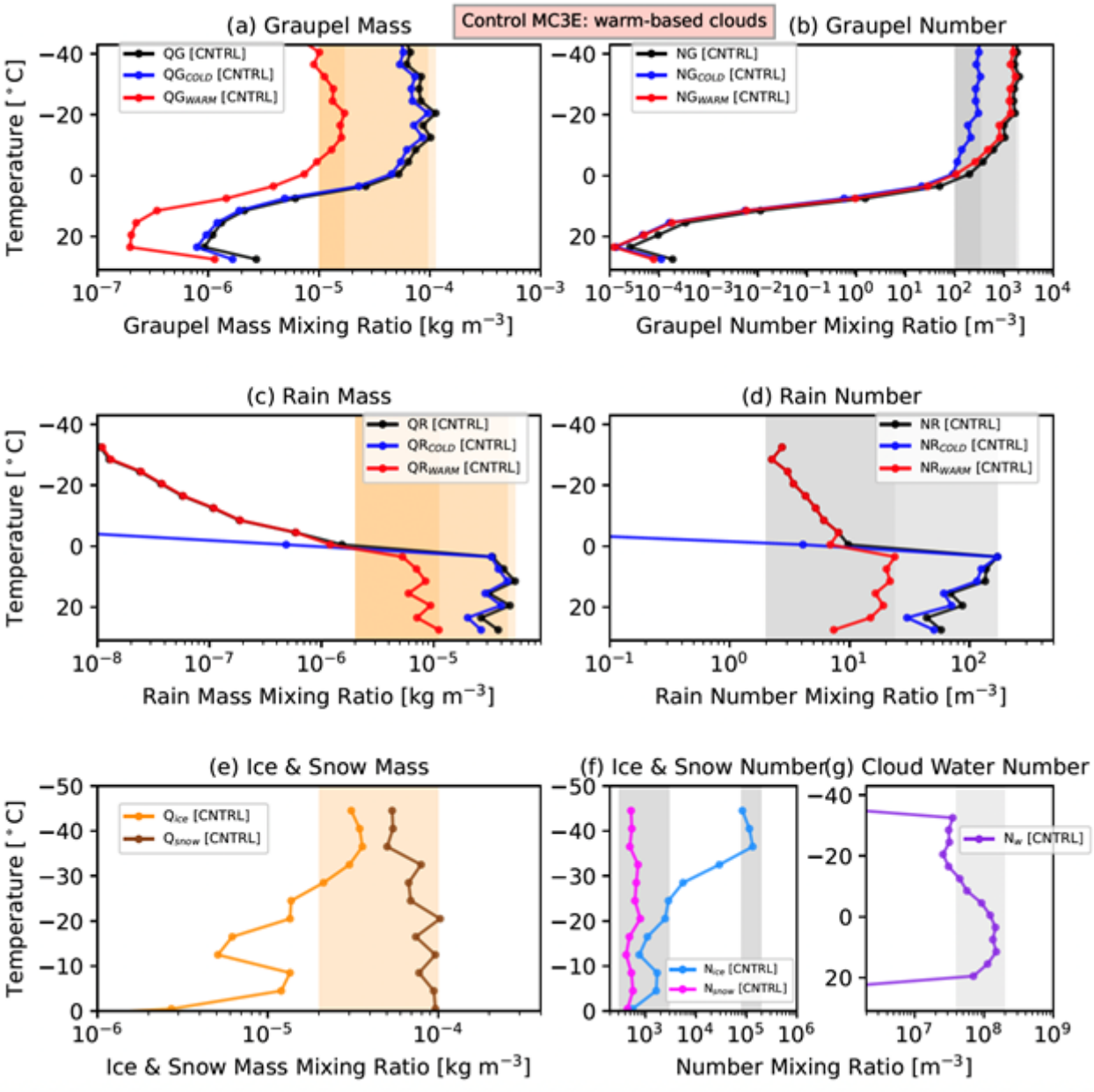

Figure 5

Same as Figure 2 but for MC3E (slightly warm-based convective clouds) during 0000–2300 UTC on 11 May 2011.

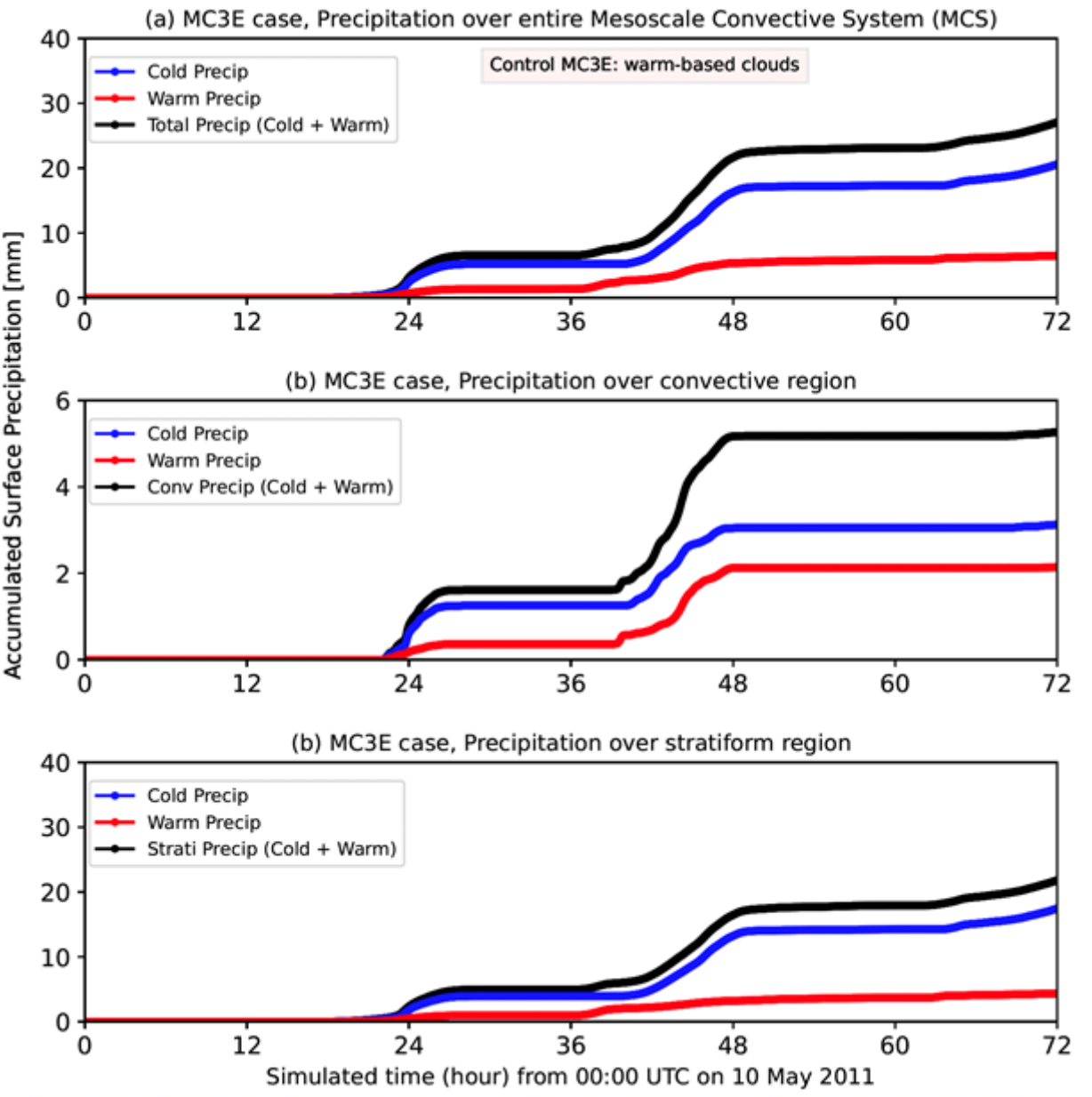

Figure 6

Same as Figure 3 but for MC3E of slightly warm-based convective clouds.

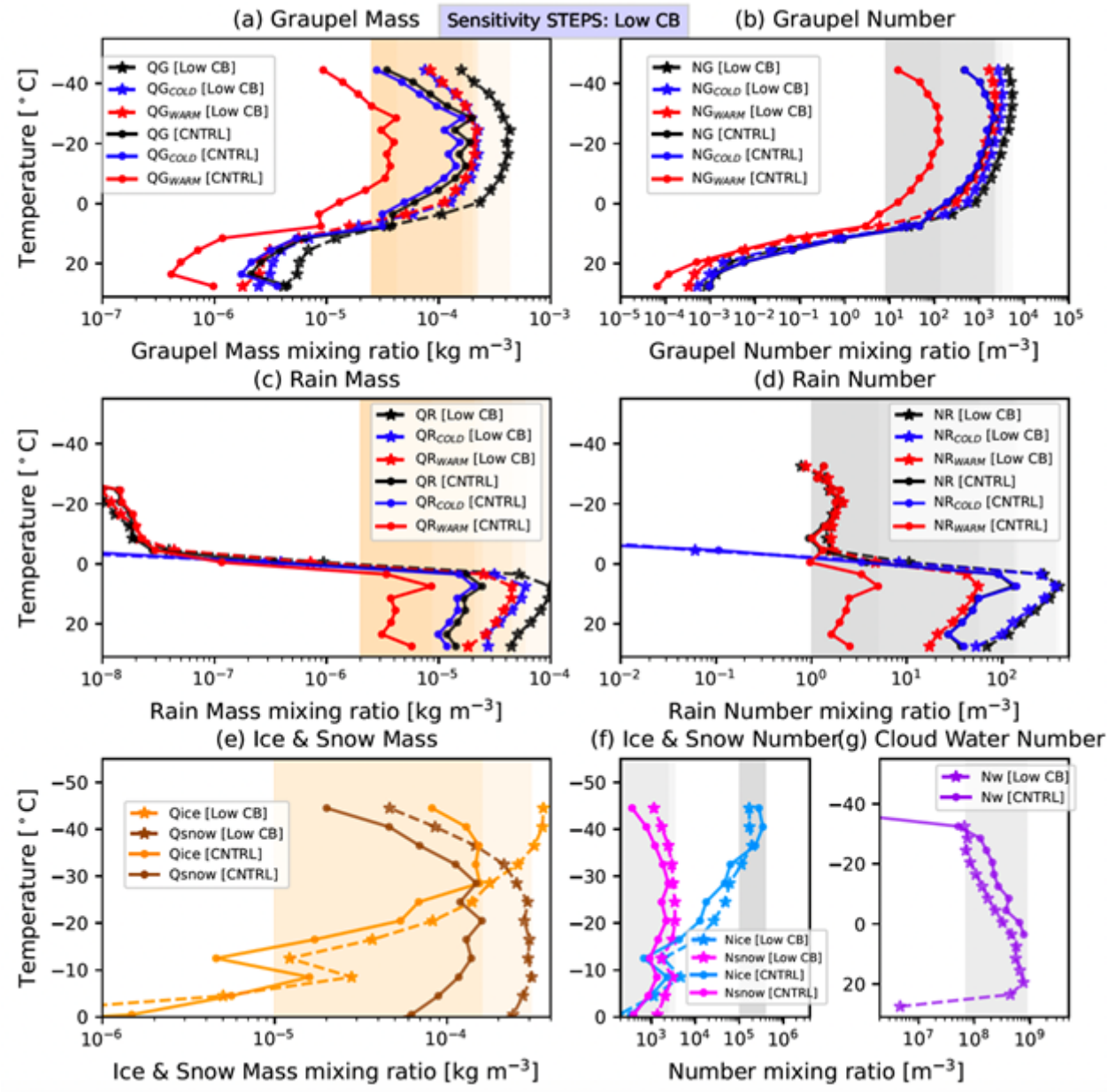

Figure 7

Same as Figure 2 but for sensitivity of different hydrometeor profiles when cloud base (Low CB) is lowered.

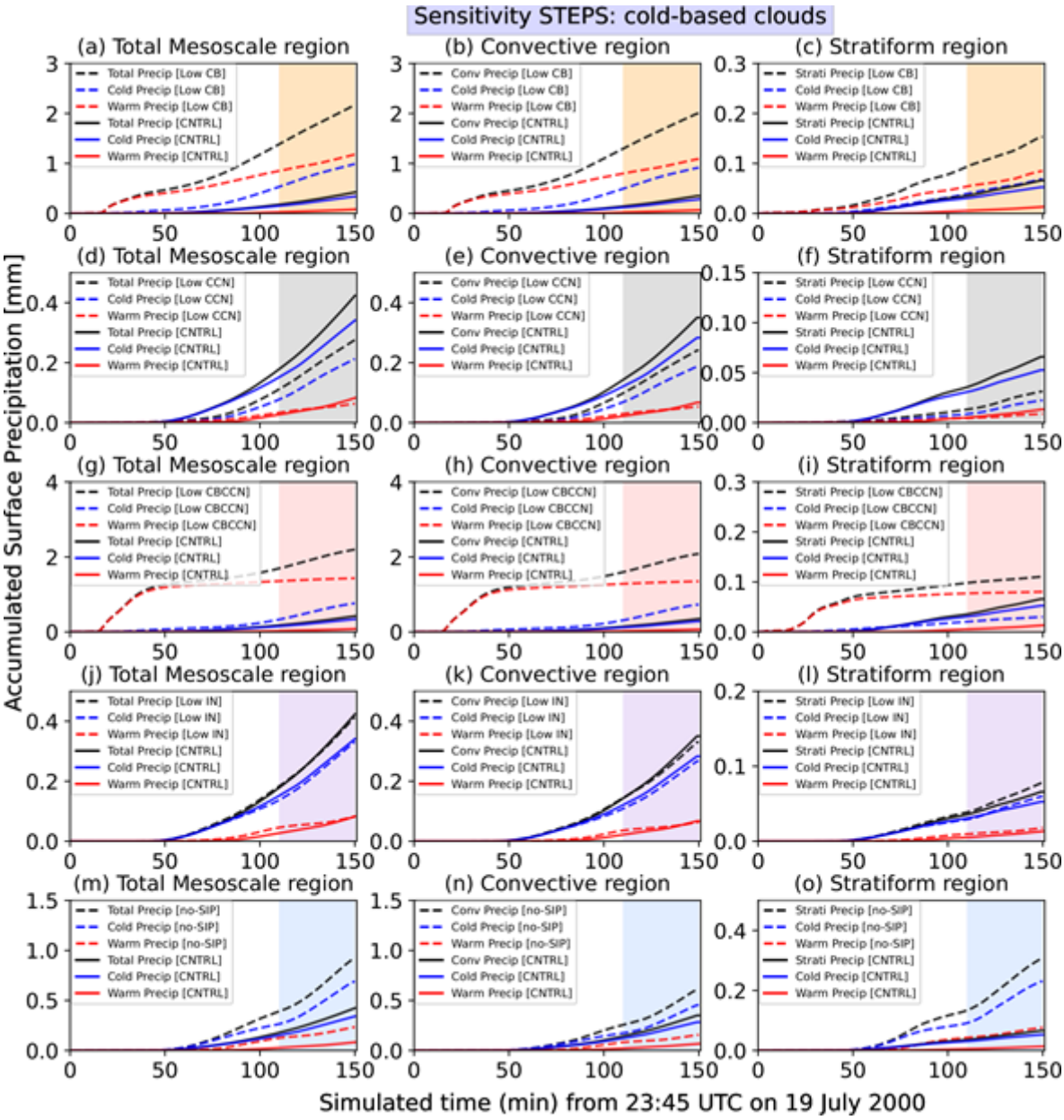

Figure 8

Simulated surface accumulation (mm) of precipitation and corresponding warm and cold components of (a) total cloudy condition; (b) convective; (c) stratiform under lowered cloud base (Low CB), (d) total; (e) convective; (f) stratiform under lowered cloud condensation nuclei (Low CCN), (g) total; (h) convective; and (i) stratiform under both lowered CB and CCN together (low CBCCN), (g) total; (e) convective; (f) stratiform under lowered ice nuclei (low IN), and (g) total; (e) convective; (f) stratiform under no secondary ice productions (no-SIP) for the STEPS case during 2345 19 June- 0215 20 June 2000. Note that the y-axis labels are different.

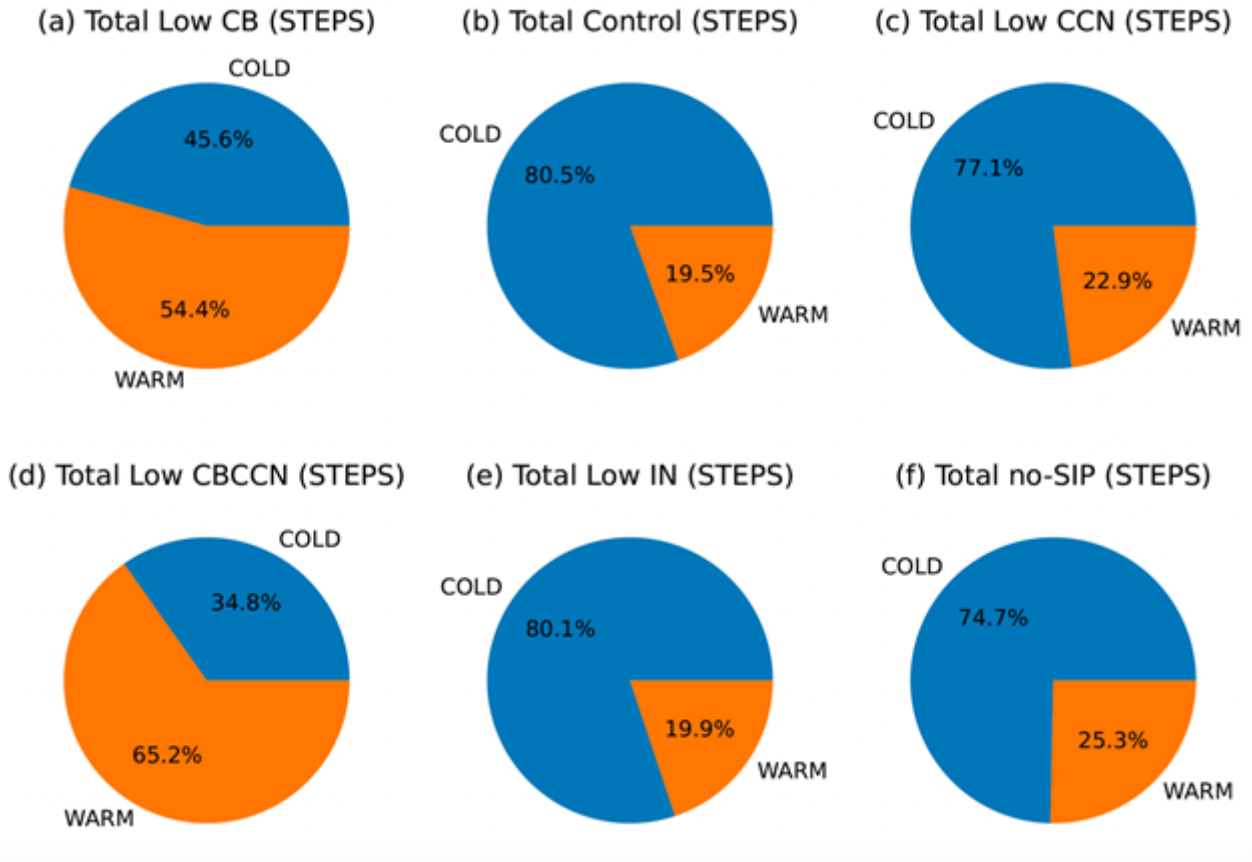

Figure 9

The pie chart depicting the fractional contribution of the warm (orange) and cold (blue) components to the total surface precipitation (a) when cloud base (CB) is lowered (low CB), (b) when simulation is run under control, (c) when CCN loading is reduced (low CCN), (d) when both CB and CCN are lowered together (low CBCCN), (e) when IN loading is lowered (low IN), and (f) when SIP is switched off (no-SIP).

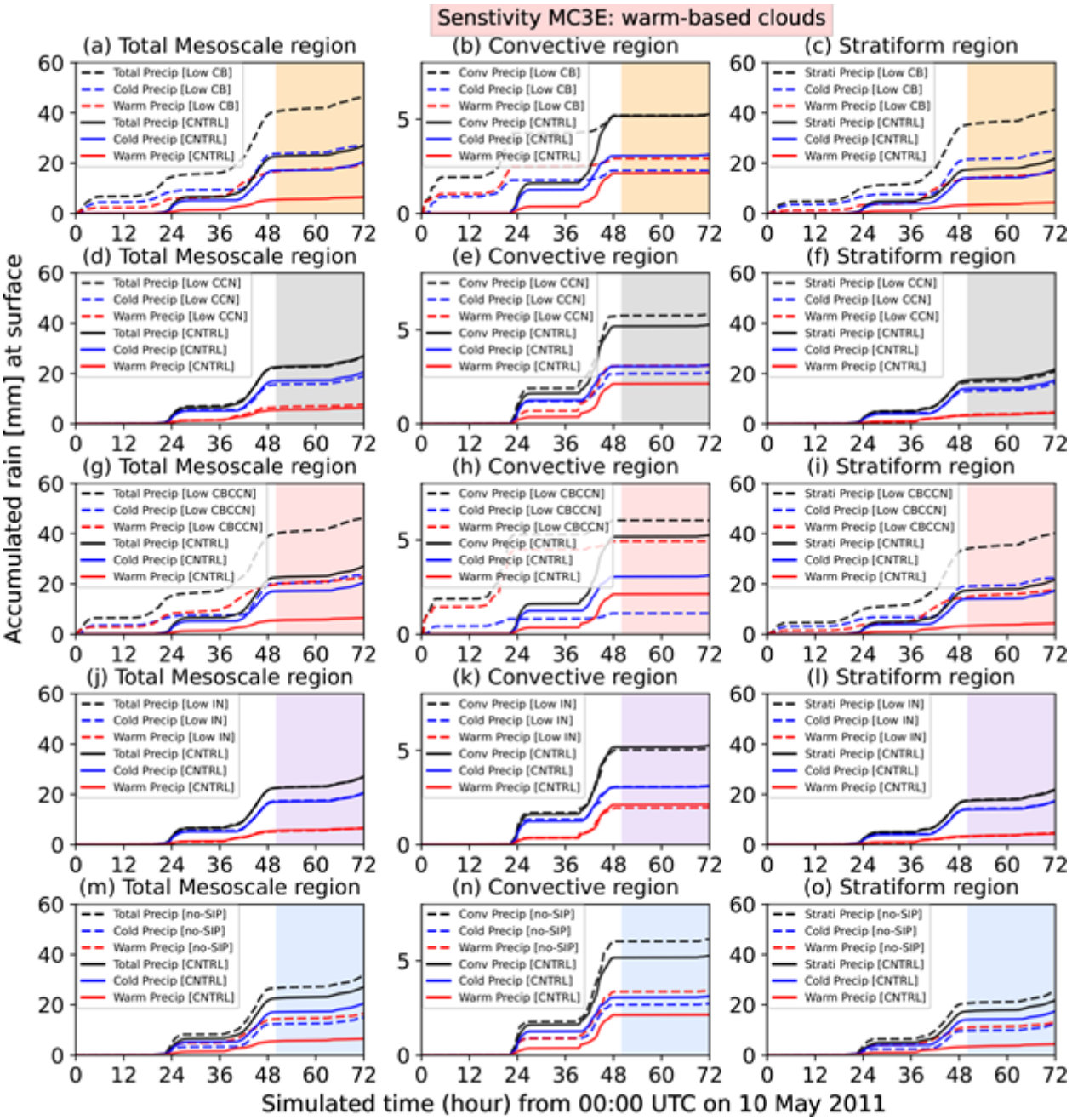

Figure 10

Same as Figure 8 but for MC3E case.

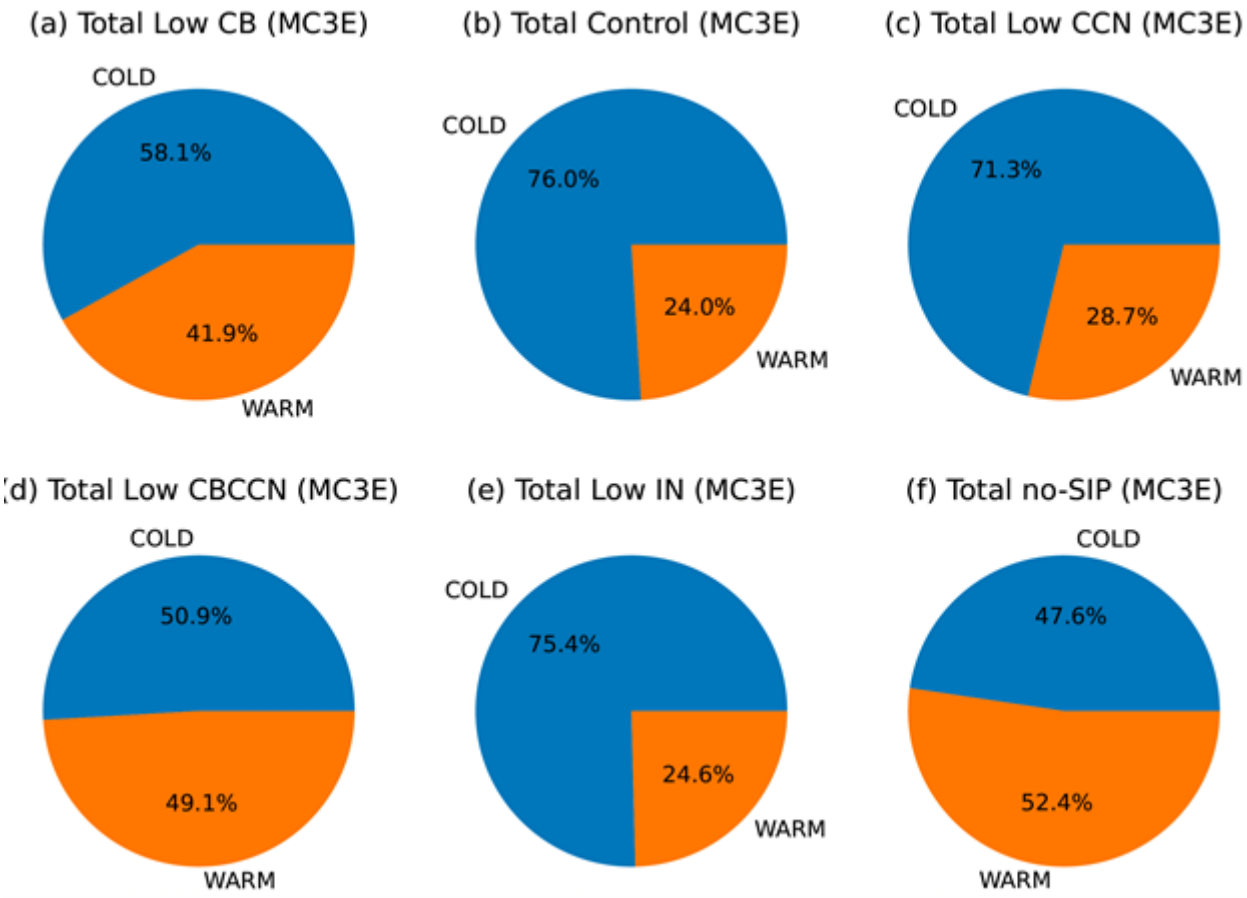

Figure 11

Same as Figure 9 but for MC3E case.

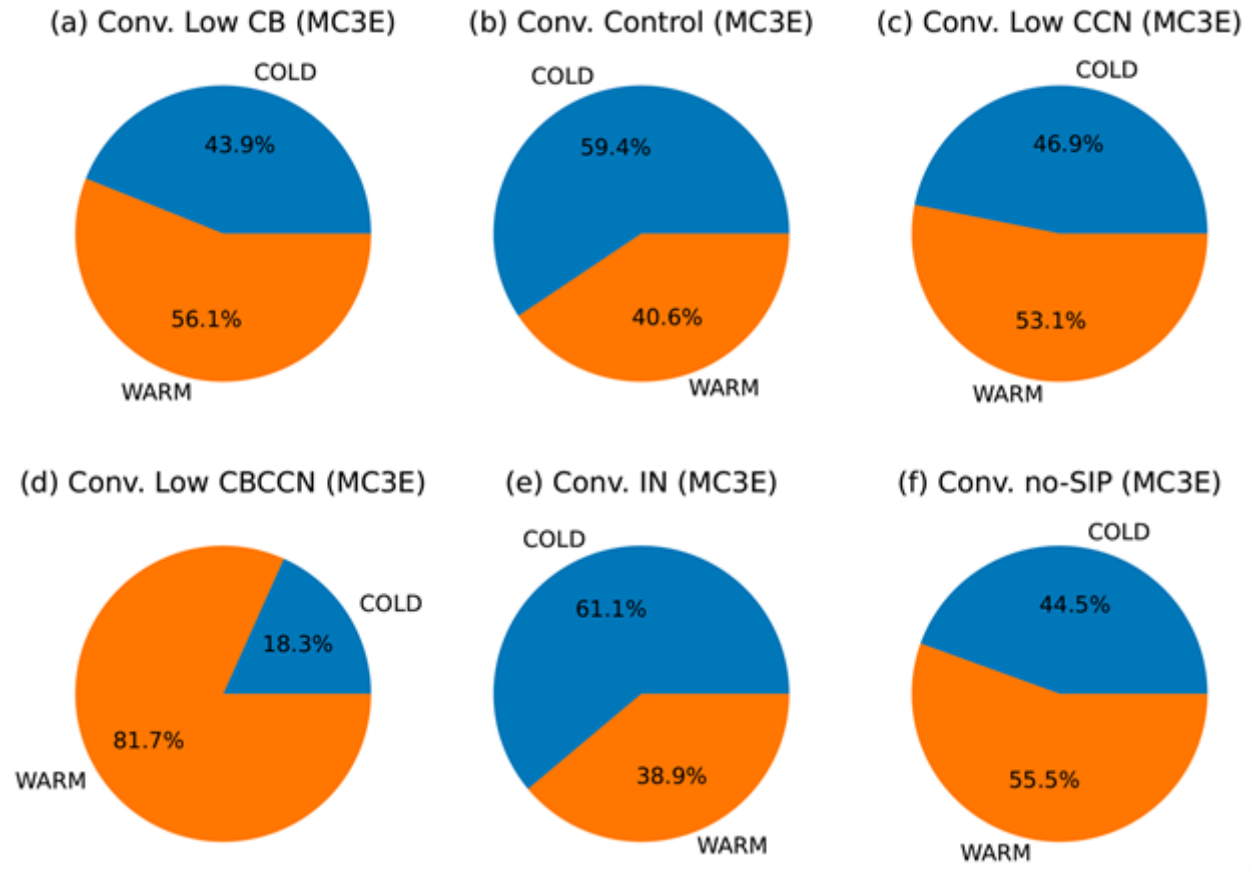

Figure 12

Same as Figure 11 but for convective case.

Supplementary Files

This is a list of supplementary files associated with this preprint. Click to download.

- SupplementaryMaterialsfor.docx